

Supporting Information

A High-Performance Dual-Functional Organic Upconversion Device with Detectivity Approaching 10^{13} Jones and Photon-to-Photon Efficiency over 20%

Zeyu He^a, Hengyuan Zhang^a, Xiaoyang Du^{a,}, Xin Yu^a, Jiayue Han^{a,b}, Luye Cao^a, Hui Lin^a, Jun Wang^{a,b}, Caijun Zheng^a and Silu Tao^{a,*}*

^aSchool of Optoelectronic Science and Engineering, University of Electronic Science and Technology of China, No.2006, Xiyuan Ave, West Hi-Tech Zone, Chengdu 610054, P.R. China

^bState Key Laboratory of Electronic Thin Films and Integrated Devices, University of Electronic Science and Technology of China, Chengdu 610054, China

* Corresponding authors. E-mail addresses: xiaoyangdu@uestc.edu.cn (X. Du), silutao@uestc.edu.cn (S. Tao).

Keywords: organic, near infrared, upconversion devices, weak light detection, pulse testing, imaging

I. Supplementary Methods

1. General information

The donor PBDB-T-2F, (Poly[(2,6-(4,8-bis(5-(2-ethylhexyl-3-fluoro)thiophen-2-yl)-benzo[1,2-b:4,5-b']dithiophene))-alt-(5,5-(1',3'-di-2-thienyl-5',7'-bis(2-ethylhexyl)benzo[1',2'-c:4',5'-c']dithiophene-4,8-dione)]) and the acceptor BTP-eC9, (2,2'-[[12,13-Bis(2-butyloctyl)-12,13-dihydro-3,9-dinonylbisthieno[2'',3'':4',5']thieno[2',3':4,5]pyrrolo[3,2-e:2',3'-g][2,1,3]benzothiadiazole-2,10-diyl]bis [methylidyne(5,6-chloro-3-oxo-1H-indene-2,1(3H)-diylidene)]bis[propanedinitrile]) were purchased from Solarmer Materials Inc. (Beijing). Chloroform (CB), the additive of 1,8-diodooctane, Zinc acetate dihydrate, ethanolamine, MoO₃ and 2-methoxyethanol were purchased from Sigma-Aldrich Inc. TAPC, TCTA, m-CBP, B3PyMPM and LiF were purchased from Xi'an p-OLED Technology Corp. All solvents were used directly as received. ITO glass was purchased from Advanced Election Technology Co., Ltd. The biological samples or sections were purchased from Suzhou Shenying Optical Co. LTD and Xinxiang Hongye edu. Instrument Co., LTD.

2. Device/Organic Films Fabrication and Methods

2.1. Experimental Section/Methods

Device Fabrication and Characterization: NIR-UCD was composed of a detection subunit and an emitting subunit and its functional layers from the bottom to the top are ZnO (20 nm)/ PBDB-T-2F: BTP-eC9 (100 nm)/ TAPC (30 nm)/ TCTA (10 nm)/ m-CBP: SAF-2NP (7% wt) (20 nm)/ B3PyMPM (45 nm). The ZnO layer was prepared on the substrate of ITO by utilizing sol-gel strategy. For detection unit, PBDB-T-2F: BTP-eC9 was mixed with weight ratio of 6:5 and was dissolved in chloroform (with 0.75% volume ratio additive of 1,8-diiodooctane) solution with a total concentration of 18 mg/ml and stirred in a glove box over 12 h and then the blending solution was prepared to be PSL film on ZnO with a speed of 4000 RPM and transferred to a hot plate immediately for thermal annealing (100°C, 10 min). After that, it was transferred to a vacuum evaporation chamber and the emission unit layer including TAPC, TCTA, m-CBP: SAF-2NP, B3PyMPM were sequentially deposited with 1 Å/s. Besides, the LiF and Al were deposited with 0.1 Å/s and 10 Å/s, respectively. The active area was square with area of 10 mm² or 1.2 cm² which was formed through the shadow mask.

Measurement Methods: The absorption spectra were tested by Hitachi U-3010 UV-VS. PL spectra were recorded by F-4600 spectrophotometer. Transient PL decay characteristics were measured with an Edinburgh Instruments FLS920 spectrometer. Horizontal dipole ratio was measured by molecular orientation analyzer (Hamamatsu C14234-11). For the experiment of photoluminescence quantum yield (PLQY) test, the solid film of m-CBP: B3PyMPM: SAF-2NP (50%:50%:7%, weight ratio) by using

deposited method was prepared with thickness of 60 nm. And then the film was excited by 310 nm light and the PLQY was tested and calculated by a PLQY testing system (HAMAMATSU, C9920-02G). The film morphology of photosensitive layer was studied via Atomic force microscope (AFM, Asylum Research AFM system (MFP-3D-BIO)) and transmission electron microscopy (TEM, Hitachi TEM system). External quantum efficiency properties of the UCDs and the detection unit were performed with a QEX10 Quantum Efficiency Measurement System. The characteristics of electron-readout of the detection unit and the NIR-UCDs were performed with a Keithley 2400 source meter instrument. The low currents and highly time-resolved photo-response characteristics of UCD were measured by a PDA semiconductor analyzer with probe station. The 1/f noise spectrum is performed by PDA 1/f noise module. The electroluminescent characteristics of emission unit and the UCD were tested by a Spectrascan PR655 photometer under ambient atmosphere. For biomedical application, the imaging laser intensity is low than 10 $\mu\text{W}/\text{cm}^2$. and at this intensity.

2.2 Fabrication of the emitting subunit

The structures of the emitting subunit is ITO/TAPC (30 nm)/TCTA (10 nm)/ m-CBP:SAF-2NP (20 nm)/B3PyMPM (45 nm)/LiF (0.8 nm)/Al (100 nm). Indium tin oxide (ITO) glass substrates with a sheet resistance of 15 Ω per square were firstly cleaned with acetone, ethanol, and deionized water, and then dried in an oven at 120 $^{\circ}\text{C}$ for 2 h. Prior to being put into the thermal deposition instrument, the substrates were treated with UV-ozone for 20 minutes. All organic films were fabricated by evaporating organic layers at a rate of 1 \AA s^{-1} onto the ITO substrate sequentially at a pressure below

3×10^{-4} Pa. Onto the electron transporting layer, a layer of LiF with 0.8 nm thickness was deposited at a rate of 0.1 \AA s^{-1} to improve electron injection. Finally, a 100-nm-thick layer of Al was deposited at a rate of 10 \AA s^{-1} as the cathode.

2.3 Fabrication of the detecting subunit

The structure of the detecting subunit of NIR-UCDs is ITO/ZnO (15 nm)/ PBDB-T-2F: BTP-eC9 (80 nm) (6:5, weight ratio)/ MoO₃ (10 nm)/Ag (150 nm). The ITO substrates were firstly cleaned using detergent, deionized water, ethyl alcohol, acetone and ethyl alcohol for every 30 min, and then treated in ultraviolet ozone for 15 min. The ZnO layer was prepared on the substrate of ITO by utilizing sol-gel strategy with annealing treatment in the atmosphere for 2 h with 200 °C to form the ZnO film. And then, a blending solution of PBDB-T-2F: BTP-eC9 was spin-coated onto ZnO with a speed of 3000~6000 RPM and with thermal annealing (100°C, 10 min), immediately. And then, the film was put into a vacuum evaporation chamber to despoide the MoO₃ with a ratio of 0.3 \AA s^{-1} and the Ag electrodes with speed of 3 \AA s^{-1} .

2.4 Fabrication of the testing film

The film samples of the m-CBP, B3PyMPM, SAF-2NP, m-CBP: B3PyMPM and m-CBP: B3PyMPM:SAF-2NP for PL and the transient PL spectrum were 30 nm thickness with depositing speed of 1 \AA s^{-1} . The ratio of the blend films of m-CBP: B3PyMPM was 1:1 and of m-CBP: B3PyMPM:SAF-2NP was (1:1:0.15), respectively. The film of the PBDB-T-2F: BTP-eC9 for AFM testing was on the ZnO substrate and is with the same fabricating method with the PSL film in the detection subunit. The film of the horizontally oriented dipoles test was a m-CBP: B3PyMPM: SAF-2NP was (1:1:0.15)

film with thickness of 20 nm, which was fabricated on a quartz glass and was encapsulated with another piece of quartz glass by using UV curing adhesive.

2.5 Measurement Details

In the horizontally oriented dipoles test, the excitation wavelength is around 380 nm and the reflection coefficient of the organic film, and the quartz glass was 1.8 and 1.55 respectively. For 77 K fluorescence and phosphorescence spectrum of the SAF-2NP, the scan speed of the measurement is 240 nm/min, and the excitation wavelengths are 380 nm. For room temperature fluorescence spectrum of the m-CBP, B3PyMPM and m-CBP: B3PyMPM: SAF-2NP film, the excitation wavelengths were 270 nm, 290 nm and 460 nm, respectively. For 77 K fluorescence and phosphorescence spectrum of the m-CBP: SAF-2NP (1:1) film, the excitation wavelength was 300 nm and the chopping speed of the phosphorescence spectrum test was 40 Hz. And we give the details of that how the pulse test works: when near-infrared light passes through a specific location in the human body, including arteries, a portion of the light is absorbed by arteries and other tissues. Because near-infrared light has good transmission ability in human tissues, another part of the light will be transmitted to our near-infrared OPD. During the test, the blood volume in the arteries changes over time, resulting in a corresponding change in the intensity of the transmitted light. Thus, the near-infrared photodiode converts changes in the photocurrent to represent the arterial pulse signal and the results are obtained.

II Supplementary Figures S1-S13

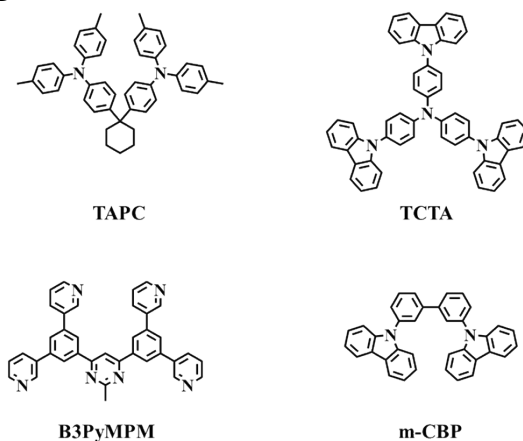


Figure S1. Materials structure of TAPC, TCTA, m-CBP and B3PyMPM.

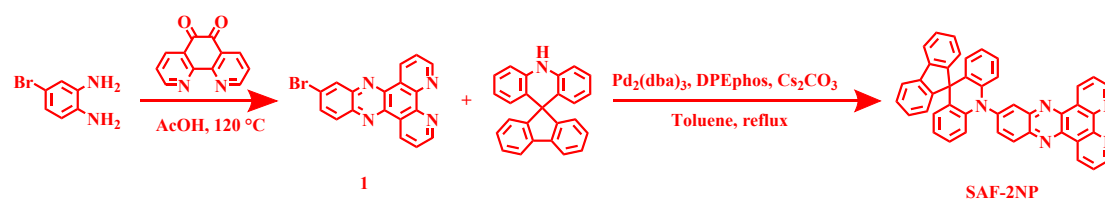


Figure S2. Schematic diagram of synthesis route of SAF-2NP.

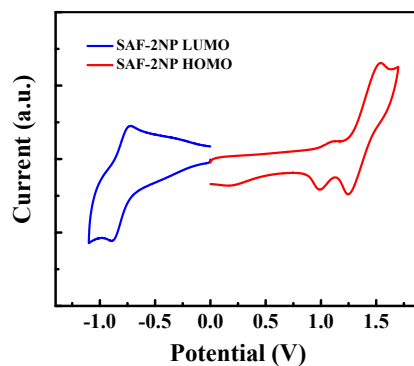


Figure S3. Oxidation and reduction curves of SAF-2NP.

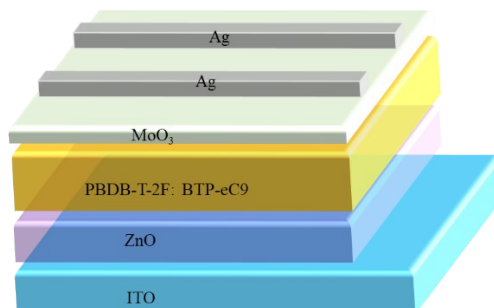


Figure S4. Device structure diagram of the detecting subunit.

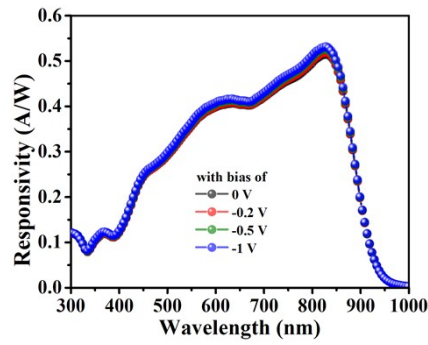


Figure S5. Responsivity curves of the detecting subunit at bias of 0, -0.2, -0.5 and -1 V, respectively.

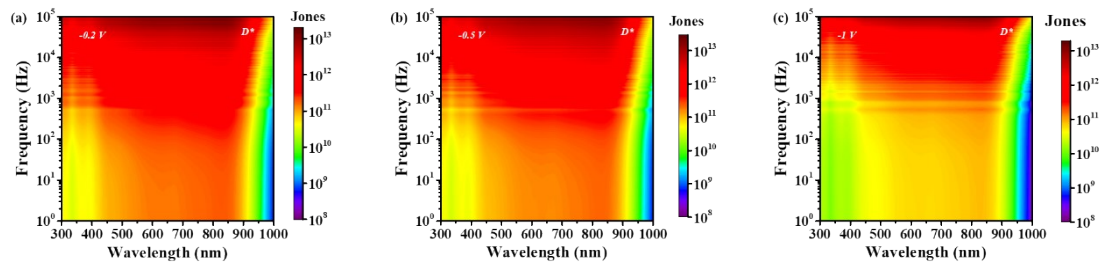


Figure S6. Specific detectivity as a function of frequency and incident light wavelength of the detecting subunit. (a) 0 V, (b) -0.5 V and (c) -1 V.

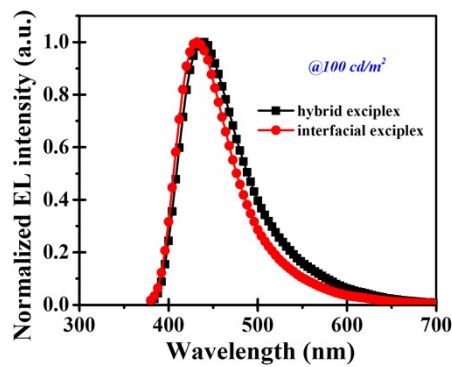


Figure S7. Normalized EL spectrum of the hybrid and the interfacial exciplex at 100 cd/m^2 .

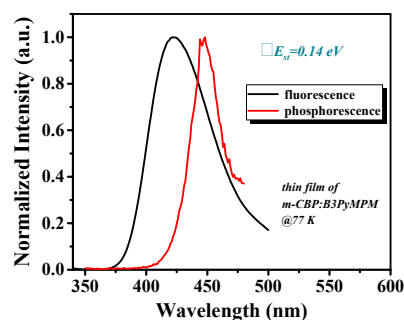


Figure S8. Normalized fluorescence and phosphorescence spectra of the m-CBP:B3PyMPM film at 77 K.

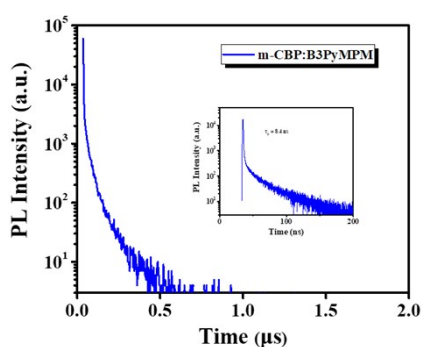


Figure S9. Transient PL spectrum of the exciplex.

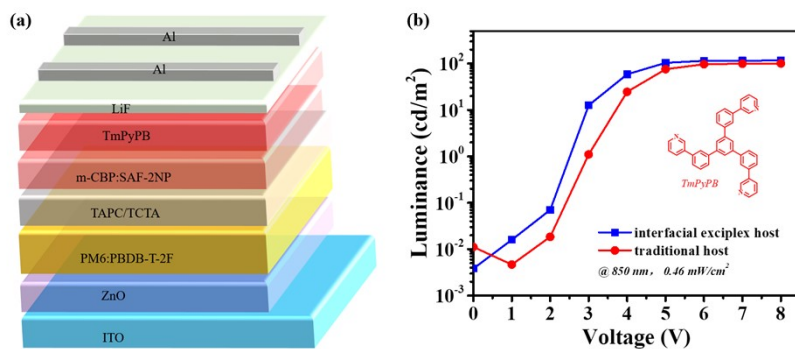


Figure S10. (a) Device structure of the control group (ITO/ ZnO/ PBDB-T-2F: BTP-eC9/ TAPC/ TCTA/ m-CBP: SAF-2NP/ TmPyPB/ LiF/ Al) and (b) Luminance-voltage curves of our device and the control group (The inset shows the molecular structure of TmPyPB).

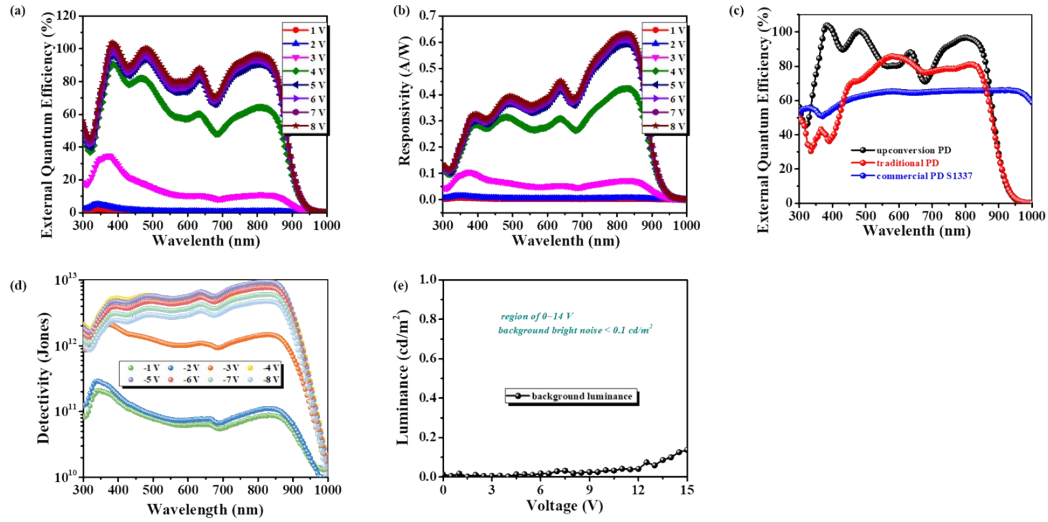


Figure S11. Performance of the NIR-UCDs. (a) External quantum efficiency of the NIR-UCDs at different bias voltages. (b) Responsivity of the NIR-UCDs at different bias voltages. (c) Responsivity of a NIR-UCD in this work, a commercial Si-based (S1337-1010BQ) photodetector and a detecting subunit. (d) Wavelength dependent detectivity of the NIR-UCDs with different bias voltages. (e) Background luminance noise testing result of the NIR-UCDs.

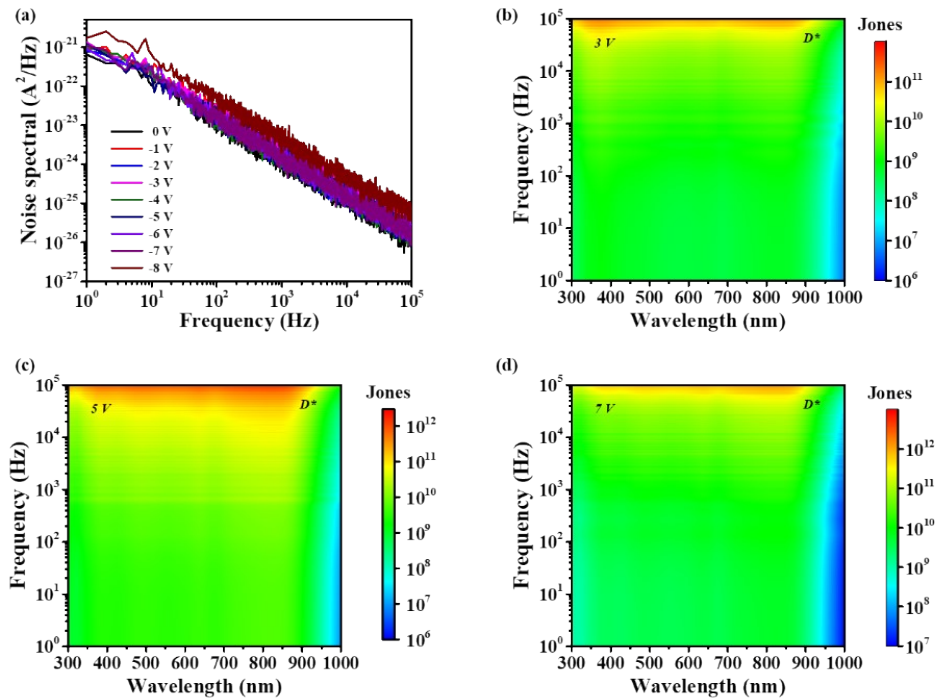


Figure 12. (a) Noise spectrum of the NIR-UCDs at different voltages. (b) Specific detectivity as a function of frequency and incident light wavelength of the detecting subunit. (b) 3 V, (c) 5 V and (d) 7 V.

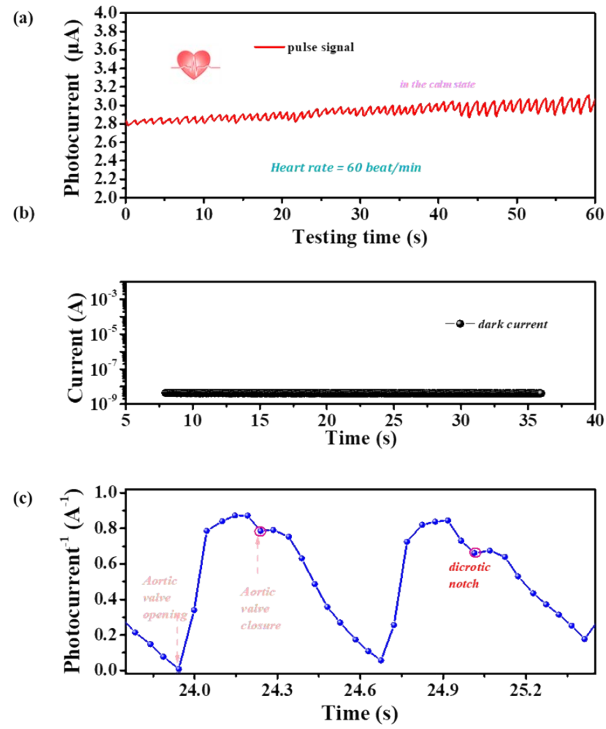


Figure S13. (a) Continuous pulse monitoring for 60 seconds when author was in the calm state. (b) Time-dependent current of the NIR-UCD when the bias is 5 V. (c) Amplified pulse signal and pulse signal analysis.

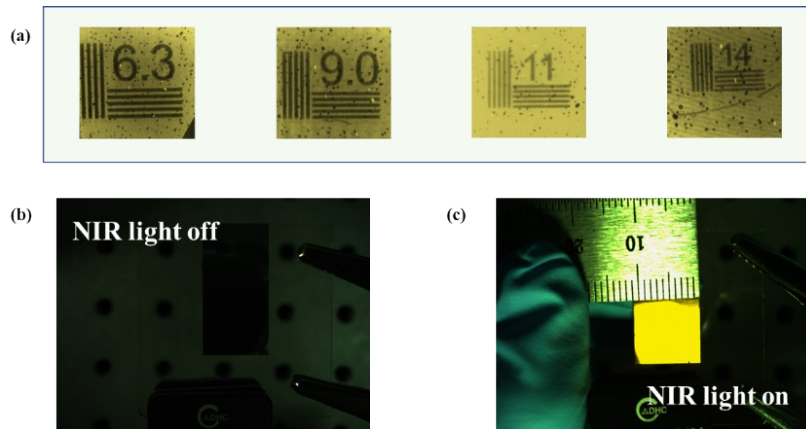


Figure S14. (a) Resolution test results using a line pair resolution test target. (b) The photograph of the NIR-UCD in the dark with bias 8 V and (c) the device sample with NIR-light irradiation under 895 nm at 8 V bias.